ADVANCED HEALTHCARE MATERIALS

Supporting Information

for *Adv. Healthcare Mater.*, DOI 10.1002/adhm.202200989

Annealing High Aspect Ratio Microgels into Macroporous 3D Scaffolds Allows for Higher Porosities and Effective Cell Migration

*Alisa C. Suturin, Andreas J. D. Krüger, Kathrin Neidig, Nina Klos, Nina Dolfen, Michelle Bund, Till Gronemann, Rebecca Sebers, Anna Manukanc, Ghazaleh Yazdani, Yonca Kittel, Dirk Rommel, Tamás Haraszti, Jens Köhler and Laura De Laporte**

Supporting Information

Annealing High Aspect Ratio Microgels into Macroporous 3D Scaffolds Allows for Higher Porosities and Effective Cell Migration

*Alisa C. Suturin, Andreas J. D. Krüger, Kathrin Neidig, Nina Klos, Nina Dolfen, Michelle Bund, Till Gronemann, Rebecca Sebers, Anna Manukanc, Ghazaleh Yazdani, Yonca Kittel, Dirk Rommel, Tamás Haraszti, Jens Köhler, Laura De Laporte**

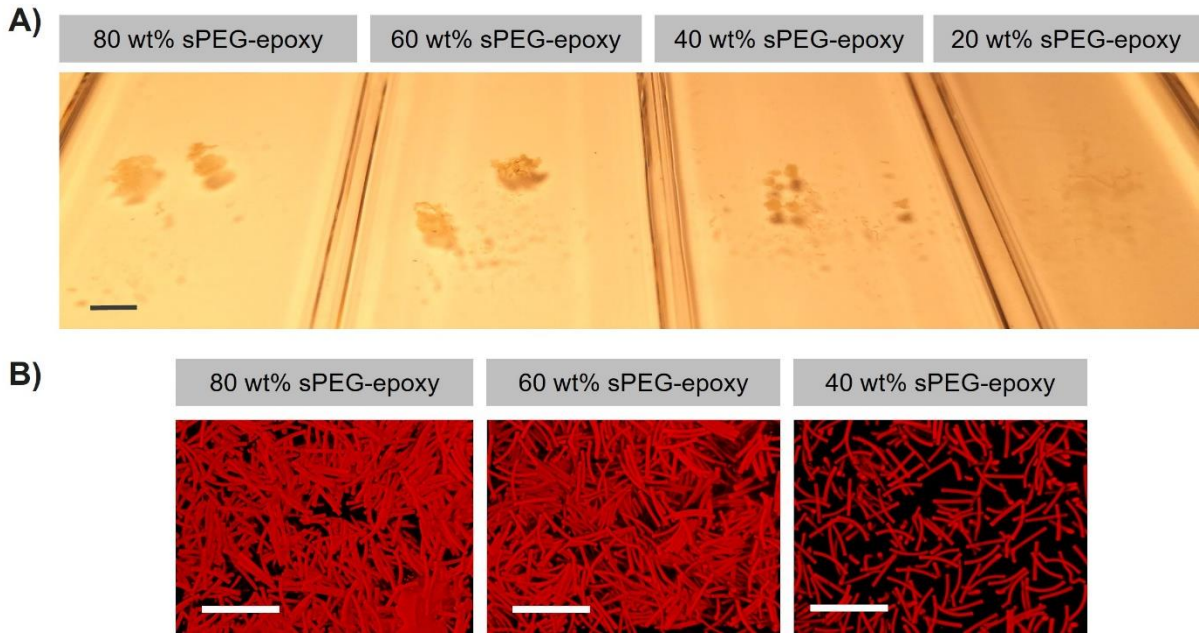

Figure S1: Stabilities of microgel assemblies depending on concentration of sPEG-epoxy solution. Annealing is performed by adding 100,000 microgel rods (10x10x100 µm³) made with 29 wt% AEMA into the aqueous solution of sPEG-epoxy. A) Macroscopic images of two scaffolds assembled in the respective sPEG-epoxy solution (20, 40, 60, or 80 wt%). Stable scaffolds are obtained for sPEG-epoxy concentrations of 60 wt% or higher. The image is recorded with a Leica dual camera. Scale bar: 5 mm. B) Confocal z-stacks images of scaffolds interlinked in different sPEG-epoxy dilutions. Scale Bar 200 µm.

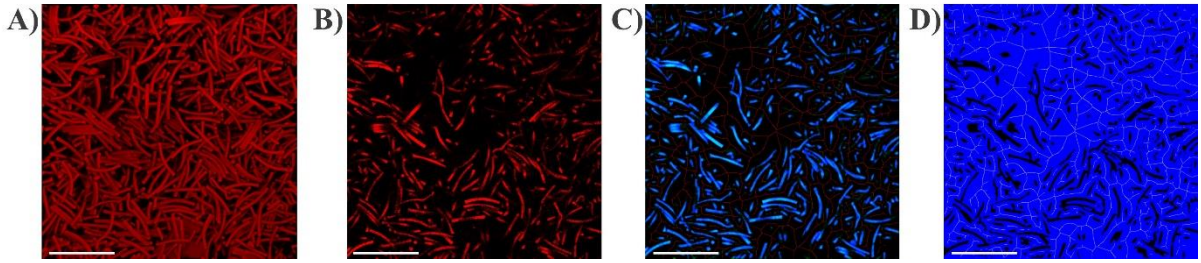

Figure S2: Analysis steps to determine porosity shown with one exemplary image. A) Z-projection of z-stack recorded using confocal microscopy. The scaffold is made from 10x10x100 µm³ dimensioned microgels containing 29 wt% AEMA. For the porosity determination, the pore sizes of each recorded z-stack slice are determined separately. B) Unprocessed single z-stack slice that will be used for determination of scaffold porosity. C) Binary overlay of the normalized scaffold image (normalized to intensities 0-255, objects shown in blue) and the applied skeleton (shown in red). D) Processed image overlay of scaffold (detected void spaces shown in blue) and skeleton shown in white. Scale bar 200 µm.

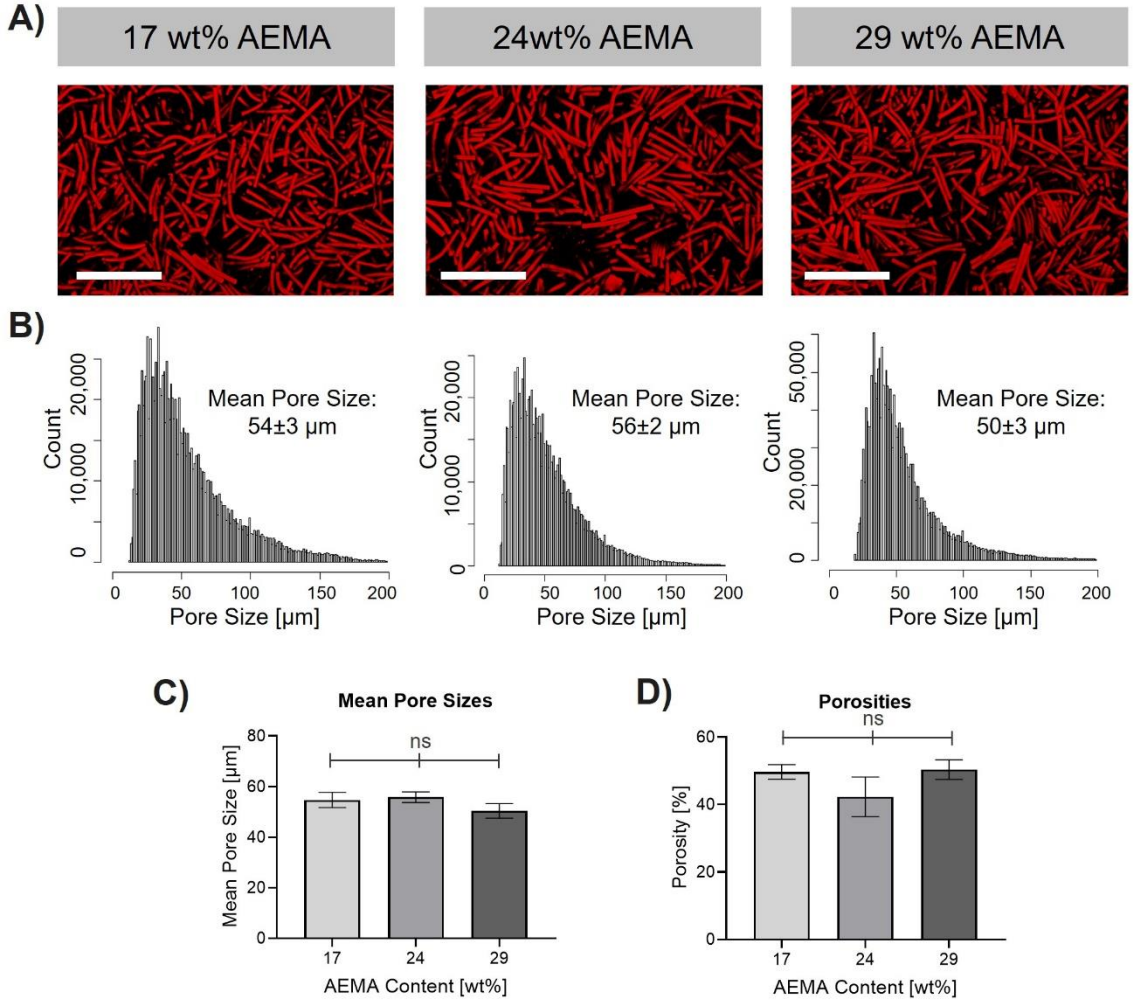

Figure S3: Influence of AEMA concentration in microgels on scaffolds pore sizes. 100,000 microgel rods (10x10x100 µm³) are interlinked via centrifugation. A) Projection images of Z-stack confocal images from MAPs made from different microgels. Scale bar 200 µm. B) The pore size distribution is obtained by analyzing z-stack confocal images with a python script and using an R-script to bin and visualize the output data. C) Comparison of scaffold mean pore sizes determined with a python script. D) Comparison of scaffold porosities determined with a python script. For both B and C, the mean out of three different scaffolds is shown (error bars represent ± SEM). *P*-values are determined using one-way ANOVA with post-hoc Tuckey's test, non-significant (ns) $p \geq 0.05$, *$p < 0.05$.

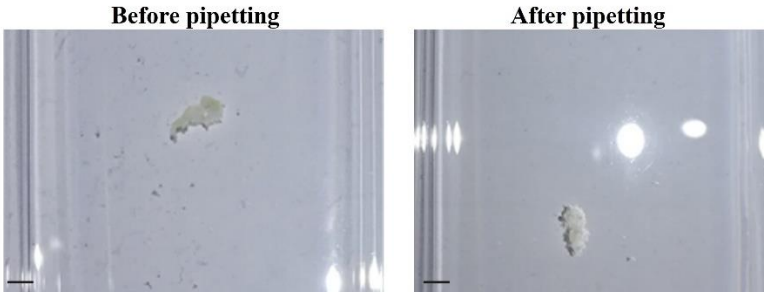

Figure S4: Mechanical integrity after pipetting MAP scaffold. Here, a 5 mL pipette is used to pipette a MAP scaffold with a total microgel volume of 0.945 mm³. Scale bar 5 mm.

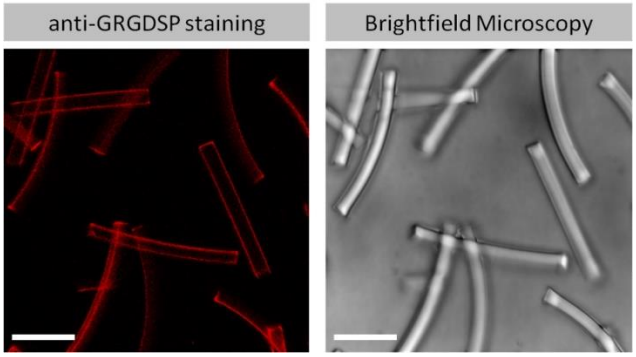

Figure S5: Microgel surface functionalized with GRGDSPC. Pre-assembly functionalized microgel rods (29 wt% AEMA, 10x10x100 µm³) are stained with anti-GRGSP primary antibody (Biorbyt, 1:100) and Alexa Fluor 568 goat anti-rabbit (Invitrogen, 1:100). Z-stack images are recorded with confocal microscopy showing RGD functionalization onto the microgel surfaces. Scale bar: 50 µm.

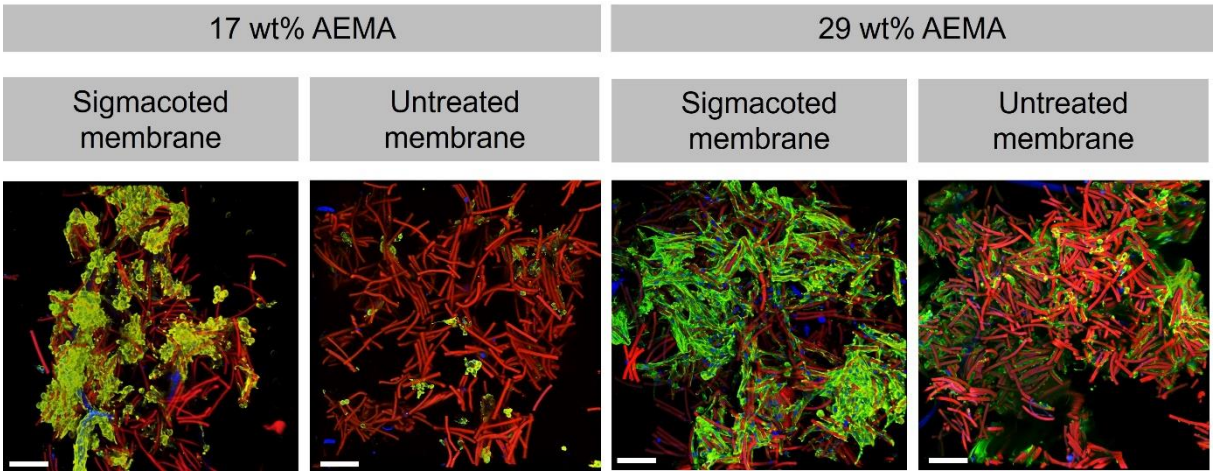

Figure S6: Influence of sigmacoting of cell culture inserts on L929 cell growth and migration after 7 d. Assemblies made from microgels (10x10x100 μm³) of different AEMA concentrations. Cells grow and spread significantly better in 3D assemblies made from microgels with 29 wt%. By sigmacoting the cell inserts, microgel scaffolds stick less to the translucent membrane bottom of the cell inserts allowing for easier transfer to glass slides for confocal microscopy. Furthermore, a more desired cell behavior is observed in scaffolds cultured in sigmacoted cell culture inserts as the coating reduces cell growth on the membrane of the cell insert. Scale bar 200 μm.

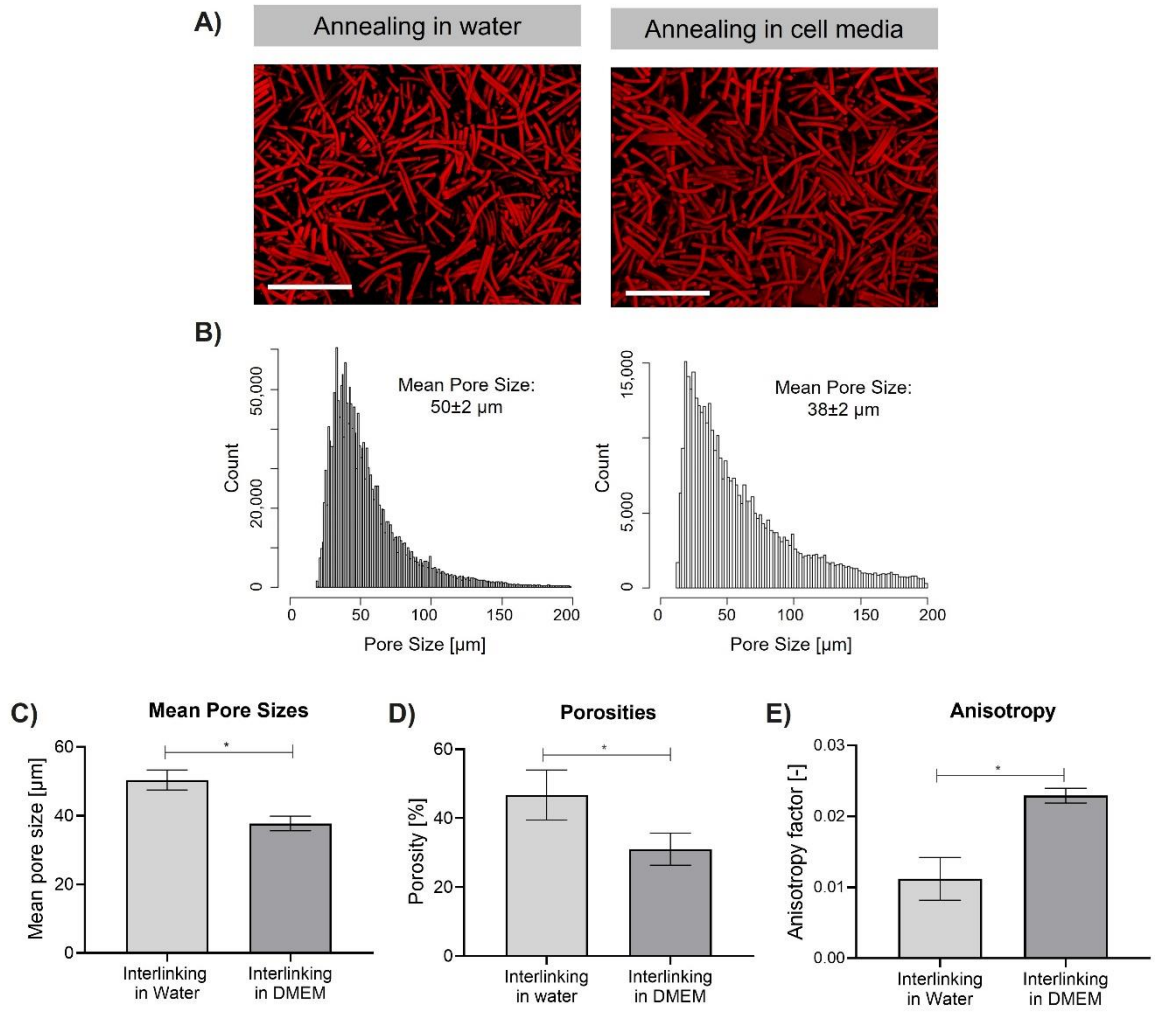

Figure S7: Influence of annealing in water or cell media on scaffolds pore characteristics. sPEG-epoxy was diluted to 60 wt% in either deionized water or supplemented DMEM. 100,000 microgel rods (10x10x100 µm³, 29 wt% AEMA) were interlinked into scaffolds. A) Z-stack confocal images showing MAPs interlinked in 60 wt% sPEG-epoxy. Scale bar 200 µm. B) The pore size distribution is obtained by analyzing z-stack confocal images with a python script and using an R-script to bin and visualize the output data. C) Comparison of scaffold mean pore sizes determined with a python script. D) Comparison of scaffold porosities determined with a python script. E) Anisotropic factor determined using ImageJ (Plugin: FibrilTool[2]). For C, D, and E, the mean out of three different scaffolds is shown (error bars represent ± SEM). *P*-values are determined using Welch's t-test for unpaired data, $*p < 0.05$.

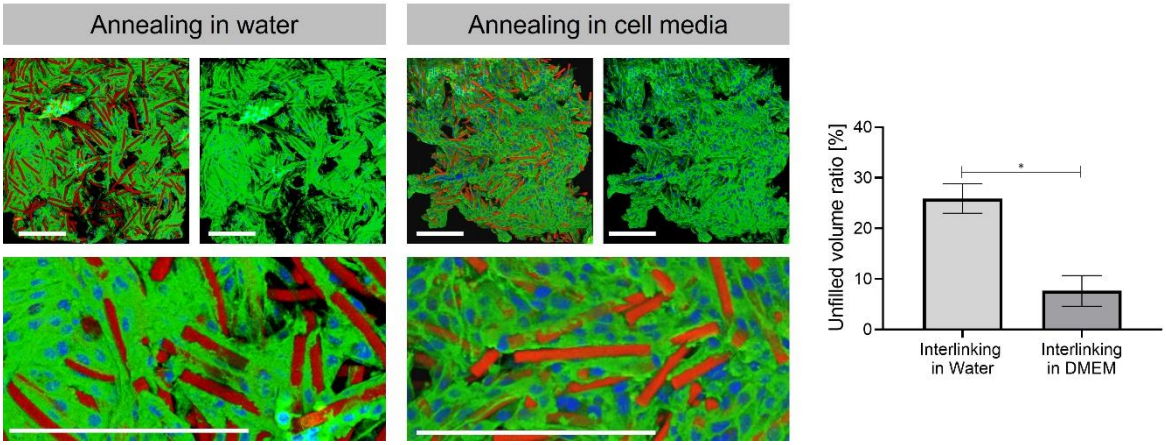

Figure S8: L929 cell growth on microgel assemblies annealed in water or cell media after 7 days of cell culture. Microgels (10x10x100 µm³) contain 29 wt% AEMA and are annealed in 60 wt% sPEG-epoxy. A) Z-stack confocal images showing MAPs. Scale bar 200 µm. B) Comparison of remaining empty volume (interstitial space in between the microgels not filled by cells) determined by analyzing respective z-projections. The mean out of three different scaffolds is shown (error bars represent ± SEM). *P*-values are determined using Welch's t-test for unpaired data, $*p < 0.05$.

Table S1. Microgel Compositions. Required masses and volumes to obtain the different microgel compositions. Final microgel compositions are given in wt/vol%.

wt% AEMA	m_{AEMA} [mg]	n_{AEMA} [mmol]	V_{filler} [µL]	$V_{PEG\text{-}DA/IRG}$ [µL]	wt% PEG-DA	$n_{PEG\text{-}DA}$ [mmol]
16.8	93.6	0.565	414	111	20.0	0.159
24.1	133.5	0.811	414	111	20.0	0.159
29.2	162.0	0.984	414	105	19.2	0.150

References

[1] a)J. C. Rose, M. Cámara-Torres, K. Rahimi, J. Köhler, M. Möller, L. De Laporte, *Nano Letters* **2017**, 17, 3782; b)A. J. D. Krüger, J. Köhler, S. Cichosz, J. C. Rose, D. B. Gehlen, T. Haraszti, M. Möller, L. De Laporte, *Chemical communications* **2018**, 54, 6943.
[2] A. Boudaoud, A. Burian, D. Borowska-Wykręt, M. Uyttewaal, R. Wrzalik, D. Kwiatkowska, O. Hamant, *Nature Protocols* **2014**, 9, 457.